

# Multiple Testing for Neuroimaging via Hidden Markov Random Field

Hai Shu, Bin Nan, Robert Koeppe, and the Alzheimer's Disease Neuroimaging Initiative \*

## Abstract

One of the important objectives that the Alzheimer's Disease Neuroimaging Initiative (ADNI) tries to achieve is to understand how the human brain changes over the course of disease progression. We consider voxel-level analysis for the  $^{18}\text{F}$ -Fluorodeoxyglucose positron emission tomography (FDG-PET) imaging study in ADNI for such a purpose. Traditional voxel-level multiple testing procedures in neuroimaging, which are mostly  $p$ -value based, often ignore the spatial correlations among neighboring voxels and thus suffer from substantial loss of power. We extend the local-significance-index based procedure, which aims to minimize the false nondiscovery rate subject to a constraint on the false discovery rate, to three-dimensional neuroimaging data using a hidden Markov random field model. A generalized expectation-maximization algorithm is proposed for estimating the model parameters. Extensive simulations show that the proposed approach is more powerful than conventional false discovery rate procedures. We apply the method to the comparison between mild cognitive impairment, a disease status with increased risk of developing Alzheimer's or another dementia, and normal controls in the ADNI's FDG-PET imaging study.

KEY WORDS: Alzheimer's disease; False discovery rate; Generalized expectation-maximization algorithm; Ising model; Local significance index; Mild cognitive impairment.

---

\*Hai Shu is Ph.D. student (E-mail: [haishu@umich.edu](mailto:haishu@umich.edu)), and Bin Nan is Professor (E-mail: [bman@umich.edu](mailto:bman@umich.edu)), Department of Biostatistics, University of Michigan, Ann Arbor, MI 48109. Robert Koeppe is Professor (Email: [koeppe@umich.edu](mailto:koeppe@umich.edu)), Department of Radiology, University of Michigan, Ann Arbor, MI 48109. The research is supported in part by NSF grant DMS-1007590 and NIH grant R01-AG036802. Data used in preparation of this article were obtained from the Alzheimer's Disease Neuroimaging Initiative (ADNI) database ([adni.loni.ucla.edu](http://adni.loni.ucla.edu)). As such, the investigators within the ADNI contributed to the design and implementation of ADNI and/or provided data but did not participate in analysis or writing of this report. A complete listing of ADNI investigators can be found at: [http://adni.loni.ucla.edu/wp-content/uploads/how\\_to\\_apply/ADNI\\_Acknowledgement\\_List.pdf](http://adni.loni.ucla.edu/wp-content/uploads/how_to_apply/ADNI_Acknowledgement_List.pdf).

# 1. INTRODUCTION

Alzheimer’s disease (AD) is the most common cause of dementia in the elderly population. The worldwide prevalence of Alzheimer’s disease was 26.6 million in 2006 and is predicted to be 1 in 85 persons by 2050 (Brookmeyer et al. 2007). Much progress has been made in the diagnosis of AD including clinical assessment and neuroimaging techniques. One such extensively used neuroimaging technique is  $^{18}\text{F}$ -Fluorodeoxyglucose positron emission tomography (FDG-PET) imaging, which can be used to evaluate the cerebral metabolic rate of glucose (CMRgl). Numerous FDG-PET studies (Nestor et al. 2003; Mosconi et al. 2005, 2008; Langbaum et al. 2009) have demonstrated significant reductions of CMRgl in brain regions in patients with AD and its prodromal stage mild cognitive impairment (MCI), compared with normal control (NC) subjects. These reduction could be used for the early detection of AD. Voxel-based multiple testing methods are common approaches to identify significant group differences in CMRgl.

In a seminal paper, Benjamini and Hochberg (1995) introduced false discovery rate (FDR) as an alternative measure of Type I error in multiple testing problems to the family-wise error rate (FWER), and demonstrated that the control of FDR is more powerful than that of FWER. We denote Benjamini and Hochberg (1995) method as BH. FDR is defined as the expected proportion of false rejections among all rejections. The false nondiscovery rate (FNR; Genovese and Wasserman 2002), the expected proportion of falsely accepted hypotheses, is the corresponding measure of Type II error. An FDR procedure is *valid* if it controls FDR at a prespecified level  $\alpha$ , and *optimal* if it has the smallest FNR among all level- $\alpha$  FDR procedures (Sun and Cai 2009). The traditional FDR procedures (Benjamini and Hochberg 1995, 2000; Genovese and Wasserman 2004) rely heavily on the assumption that the test statistics are independent, which rarely holds in practice. Although these approaches are shown to be valid under certain dependence assumptions (Benjamini and Yekutieli 2001; Farcomeni 2007; Wu 2008), they may suffer from severe loss of power when the dependence structure is ignored (Yekutieli and Benjamini 1999; Genovese et al. 2006; Benjamini and Heller 2007; Sun and Cai 2009). Even under independence, the local FDR (LfdR) procedure is optimal and thus more powerful than those  $p$ -value based

traditional procedures (Efron 2007; Sun and Cai 2007). Modeling the dependence structure using the hidden Markov chain (HMC) method, Sun and Cai (2009) proposed an optimal oracle procedure based on a new test statistic, the local index of significance (LIS), and corresponding asymptotic data-driven procedure. Following the work of Sun and Cai (2009), Wei et al. (2009) developed a pooled LIS (PLIS) procedure for multiple-group analysis where different groups have different HMC dependence structures, and proved the optimality of the PLIS procedure. Either the LIS procedure or the PLIS procedure only handles the one-dimensional dependency. However, problems with higher dimensional dependence are of particular practical interest. For example, Li et al. (2010) implemented the LIS procedure for genome-wide association studies.

FDR procedures have been widely used in analyzing functional neuroimaging data (Genovese et al. 2002; Nichols and Hayasaka 2003; Chumbley and Friston 2009, among many others). The current version of the well-known functional neuroimaging software Statistical Parametric Mapping (SPM), SPM8, contains both the BH procedure at the voxel level and the topological FDR procedures (Chumbley and Friston 2009; Chumbley et al. 2010) that control the FDR of clusters or peaks in a way that takes into account the spatial structure among voxels. We focus on the voxel-level FDR procedures in this article by developing a LIS-based FDR procedures for three-dimensional (3D) image data using a hidden Markov random field model (HMRF) for the spatial dependency among multiple tests.

HMRF model is a generalization of HMC model, which replaces the underlying Markov chain by Markov random field. In particular, the Ising model, a classical Markov random field, has been used to capture the spatial structure in imaging analysis (Bremaud 1999; Winkler 2003). In this article, we consider the Brodmann's participation of the cerebral cortex and subcortical regions of the human brain (Garey 2006). We assume that the unobservable states of voxels in a region on lattice  $S$  of the image grid,  $\Theta = \{\Theta_s : s \in S\}$ , follow a two-parameter Ising model, where  $\Theta_s = 1$  if there is a signal at voxel  $s$  (i.e., hypothesis  $s$  is nonnull), and  $\Theta_s = 0$  otherwise. The observed data, test statistics  $\mathbf{X} = \{X_s : s \in S\}$ , are independently generated from the standard normal distribution under the null, and a normal mixture under the nonnull. This HMRF model is a natural extension of the HMC model of Sun and

Cai (2009).

A major difficulty in estimating parameters in an HMRF model is the intractable computation of the normalizing constant in the underlying distribution. To avoid the difficulty, Chalmond (1989) used the pseudo-likelihood method proposed by Besag (1974) to approximate the likelihood as a product of tractable conditional distributions. However, Geyer and Thompson (1992) pointed out that the pseudo-likelihood method may seriously overestimate the dependence. Zhang (1992) introduced the mean field theory from statistical mechanics (Chandler 1987) to solve the intractable problem, which turns out to be a generalized pseudo-likelihood that is sensitive to noise (Marroquin et al. 2003). Both the algorithms of Chalmond (1989) and Zhang (1992) are based on the expectation-maximization (EM) algorithm (Dempster et al. 1977). Alternatively, Zhu et al. (2007) proposed the stochastic approximation EM algorithm for HMRFs based on maximum-likelihood estimation (MLE). Despite incorporating EM in the name, the algorithm is a gradient-type optimization per se, where the first- and second-order partial derivatives of the log-likelihood of the observed data are approximated by Monte Carlo averages, and unfortunately, the algorithm is restricted to the model where the conditional density  $P(\mathbf{X}|\Theta)$  belongs to the exponential family.

We propose an EM-type algorithm to search for MLE or penalized MLE (Ridolfi 1997; Ciuperca et al. 2003) that prevents the degeneracy of MLE, and use Monte Carlo averages via Gibbs sampler (Geman and Geman 1984; Roberts and Smith 1994; Gilk et al. 1996) to overcome the intractability. In the M-step, we adapt a backtracking line search method in each iteration (Nocedal and Wright 2006) to find a point that increases the objective function, leading our algorithm to be a generalized EM algorithm (GEM; Dempster et al. 1977). Then the LIS-based FDR procedures can be conducted by plugging in the estimates of the HMRF parameters.

The motivating FDG-PET image data are obtained from the Alzheimer’s Disease Neuroimaging Initiative (ADNI) database (<http://adni.loni.ucla.edu/>). These are the baseline FDG-PET images of 403 subjects, including 102 NC subjects, 206 MCI patients, and 95 AD patients. Each subject’s baseline FDG-PET image has been reoriented into a standard  $160 \times 160 \times 96$  voxel image grid with 1.5 mm cubic voxels and the anterior-posterior axis of the subject is parallel to the line connecting the

anterior and posterior commissures, so-called AC-PC line (Wang 2013). We focus on the comparison between MCI and NC, where the signals are the weakest among all three comparisons of the three groups. We consider 46 Brodmann areas and 15 subcortical regions of interest that are pre-defined for their anatomical and functional differences and commonly used in AD studies, where left and right regions sharing the same border in the middle of the brain are combined. Each image is normalized by the average of voxel values in pons and cerebellar vermis, which are well preserved regions in Alzheimer’s patients. The PLIS procedure by pooling all regions will be conducted to control the global FDR of the voxel-based multiple tests.

The article is organized as follows. In Section 2, we introduce the HMRF model, Ising model in particular, for 3D image data. We provide the GEM algorithm for the HMRF parameter estimation and the implementation of the HMRF LIS-based data-driven procedures in Section 3. In Section 4, we conduct extensive simulation studies to compare the LIS-based procedures with conventional FDR methods. In Section 5, we apply the PLIS procedure to the ADNI FDG-PET image data, which finds more signals than the conventional methods.

## 2. A HIDDEN MARKOV RANDOM FIELD MODEL

Let  $S$  be a finite lattice of  $N$  voxels in an image grid, usually in a three-dimensional space. Let  $\Theta = \{\Theta_s \in \{0, 1\} : s \in S\}$  denote the set of latent states for multiple testing in  $S$ , where  $\Theta_s = 1$  if hypothesis  $s$  is nonnull and  $\Theta_s = 0$  otherwise. Suppose  $\Theta$  be generated from a two-parameter Ising model with the following probability distribution

$$\begin{aligned}
 P_\varphi(\boldsymbol{\theta}) &= \frac{1}{Z(\varphi)} \exp\{\varphi^T H(\boldsymbol{\theta})\} \\
 &= \frac{1}{Z(\beta, h)} \exp\left\{ \beta \sum_{\langle s, t \rangle} \theta_s \theta_t + h \sum_{s \in S} \theta_s \right\}, \tag{1}
 \end{aligned}$$

where  $Z(\varphi)$  is the normalizing constant,  $\varphi = (\beta, h)^T$ ,  $H(\boldsymbol{\theta}) = (\sum_{\langle s, t \rangle} \theta_s \theta_t, \sum_{s \in S} \theta_s)^T$ , and  $\langle s, t \rangle$  denotes all the pairs  $(s, t)$  in  $S$  with  $\langle s, t \rangle = \langle t, s \rangle$  such that for any  $s$ ,  $t$  is among the six nearest neighbors of voxel  $s$ . This model possesses the Markov

property:

$$\begin{aligned} P_\varphi(\theta_s | \boldsymbol{\theta}_{S \setminus \{s\}}) &= P_\varphi(\theta_s | \boldsymbol{\theta}_{\mathcal{N}(s)}) \\ &= \frac{\exp\{\theta_s(\beta \sum_{t \in \mathcal{N}(s)} \theta_t + h)\}}{1 + \exp\{\beta \sum_{t \in \mathcal{N}(s)} \theta_t + h\}}, \end{aligned} \quad (2)$$

where  $S \setminus \{s\}$  denotes the set  $S$  after removing  $s$ , and  $\mathcal{N}(s) \subset S$  is the nearest neighborhood of  $s$  in  $S$ .

For the above Ising model, it can also be shown that

$$\begin{aligned} &\log \left\{ \frac{P(\Theta_s = 1, \Theta_t = 1 | \boldsymbol{\theta}_{S \setminus \{s,t\}})}{P(\Theta_s = 1, \Theta_t = 0 | \boldsymbol{\theta}_{S \setminus \{s,t\}})} \right. \\ &\quad \left. \times \frac{P(\Theta_s = 0, \Theta_t = 0 | \boldsymbol{\theta}_{S \setminus \{s,t\}})}{P(\Theta_s = 0, \Theta_t = 1 | \boldsymbol{\theta}_{S \setminus \{s,t\}})} \right\} \\ &= \begin{cases} \beta, & t \in \mathcal{N}(s), \\ 0, & \text{otherwise.} \end{cases} \end{aligned} \quad (3)$$

Therefore, if  $s$  and  $t$  are neighbors,  $\beta$  is equal to a log odds ratio that describes the association between  $\Theta_s$  and  $\Theta_t$  conditional on all the other state variables being withheld. We can see that  $\beta$  reflects how likely the same-state voxels are clustered together. Similarly,

$$\log \left\{ \frac{P(\Theta_s = 1 | \sum_{t \in \mathcal{N}(s)} \Theta_t = 0)}{P(\Theta_s = 0 | \sum_{t \in \mathcal{N}(s)} \Theta_t = 0)} \right\} = h,$$

which is the log odds for  $\Theta_s = 1$  given that  $\boldsymbol{\Theta}_{\mathcal{N}(s)}$  are all zero. We thus generally assume  $\beta \geq 0$  and  $h \leq 0$  accounting for the nonnegative dependency of neighboring voxels that have the same state. In addition, for a voxel  $s$  with  $m$  nearest neighbors, we have

$$\begin{aligned} &\log \left\{ \left( \frac{P(\Theta_s = 1 | \sum_{t \in \mathcal{N}(s)} \Theta_t = n)}{P(\Theta_s = 0 | \sum_{t \in \mathcal{N}(s)} \Theta_t = n)} \right) \right. \\ &\quad \left. / \left( \frac{P(\Theta_s = 0 | \sum_{t \in \mathcal{N}(s)} \Theta_t = m - n)}{P(\Theta_s = 1 | \sum_{t \in \mathcal{N}(s)} \Theta_t = m - n)} \right) \right\} \\ &= m\beta + 2h, \end{aligned} \quad (4)$$

where  $n$  is an integer satisfying  $0 \leq n \leq m$ , which reflects the log ratio of the cluster effect of signals (nonnulls) relative to the cluster effect of noises (nulls).

Conditional on  $\Theta$ , we assume that the observed test statistics  $\mathbf{X} = \{X_s : s \in S\}$  are independent with

$$P_\phi(\mathbf{x}|\boldsymbol{\theta}) = \prod_{s \in S} P_\phi(x_s|\theta_s), \quad (5)$$

where  $P_\phi(x_s|\theta_s)$  denotes the following distribution

$$X_s|\Theta_s \sim (1 - \Theta_s)N(0, 1) + \Theta_s \sum_{l=1}^L p_l N(\mu_l, \sigma_l^2) \quad (6)$$

with unknown parameters  $\phi = \{\mu_l, \sigma_l^2, p_l : l = 1, 2, \dots, L\}$ . Here we assume that the test statistic  $X_s$  follows the standard normal distribution under the null, and the nonnull distribution is set to be the normal mixture that can be used to approximate a large collection of distributions (Magder and Zeger 1996; Efron 2004). The number of components  $L$  in the nonnull distribution may be selected by, for example, the Akaike or Bayesian information criterion. Following the recommendation of Sun and Cai (2009), we use  $L = 2$  for the ADNI imaging analysis.

Markov random fields (MRFs; Bremaud 1999) are a natural generalization of Markov chains (MCs), where the time index of MC is replaced by the space index of MRF. It is well known that any one-dimensional MC is an MRF, and any one-dimensional stationary finite-valued MRF is proved to be a MC (Chandgotia et al. 2014). When  $S$  is taken to be one-dimensional, then the above approach based on (1), (5) and (6) reduces to the HMC method of Sun and Cai (2009).

### 3. HIDDEN MARKOV RANDOM FIELD LIS-BASED FDR PROCEDURES

Sun and Cai (2009) developed a compound decision theoretic framework for multiple testing under HMC dependence and proposed LIS-based oracle and data-driven testing procedures that aim to minimize the FNR subject to a constraint on FDR. We extend these procedures under HMRF for imaging data. The oracle LIS for hypothesis  $s$  is defined as  $LIS_s(\mathbf{x}) = P_\Phi(\Theta_s = 0|\mathbf{x})$  for given  $\Phi$ . Let  $LIS_{(1)}(\mathbf{x}), \dots, LIS_{(N)}(\mathbf{x})$  be the ordered LIS values and  $\mathcal{H}_{(1)}, \dots, \mathcal{H}_{(N)}$  the corresponding null hypotheses. The

oracle testing procedure operates as follows: For a prespecified FDR level  $\alpha$ ,

$$\text{let } k = \max \left\{ i : \frac{1}{i} \sum_{j=1}^i LIS_{(j)}(\mathbf{x}) \leq \alpha \right\};$$

then reject all  $\mathcal{H}_{(i)}$ ,  $i = 1, \dots, k$ . (7)

Parameters  $\Phi$  are unknown in practice. We can use the data-driven testing procedure that simply replaces  $LIS_{(i)}(\mathbf{x})$  in (7) with  $\widehat{LIS}_{(i)}(\mathbf{x}) = P_{\hat{\Phi}}(\Theta_s = 0|\mathbf{x})$ , where  $\hat{\Phi}$  is an estimate of  $\Phi$ .

If all the tests are partitioned into multiple groups and each group follows its own HMRF, in contrast to the separated LIS (SLIS) procedure that conducts the LIS-based FDR procedure separately for each group at the same FDR level  $\alpha$  and then combines the testing results, we follow Wei et al. (2009) to propose a pooled LIS (PLIS) procedure that is more efficient in reducing the global FNR. The PLIS follows the same procedure as (7), but with  $LIS_{(1)}, \dots, LIS_{(N)}$  being the ordered test statistics from all groups.

Note that the model homogeneity, which is required in Sun and Cai (2009) and Wei et al. (2009) for HMCs, fails to hold for the HMRF model, i.e., the Bernoulli distributions of the unobservable latent states are different between the interior voxels who have six nearest neighbors and the boundary voxels who have less than six nearest neighbors. Using a weighted average conditional distribution of test statistics in Sun and Cai (2009) by incorporating the individual bernoulli probability as weight, one can show that the same theoretical results for the oracle procedures in Sun and Cai (2009) and Wei et al. (2009) also hold for the HMRF model.

We now provide details of the LIS-based data-driven procedure for 3D imaging data. First of all, the parameters of the HMRF model need to be estimated from observed test data.

### 3.1 A Generalized EM Algorithm

We propose an EM approach for the estimation of parameters in the HMRF model characterized by (1), (5) and (6) by maximizing the observed likelihood function  $L(\Phi|\mathbf{x}) = P_{\Phi}(\mathbf{x})$ . We first introduce unobservable categorical variables  $\mathbf{K} = \{K_s : s \in S\}$  such that  $P(K_s = 0|\Theta_s = 0) = 1$ ,  $P(K_s = l|\Theta_s = 1) = p_l$  and  $P(X_s =$



$x_s|\Theta_s, K_s) = N(\mu_{K_s}, \sigma_{K_s}^2)$ , where  $K_s \in \{0\}\mathbf{1}(\Theta_s = 0) + \{l = 1, \dots, L\}\mathbf{1}(\Theta_s = 1)$  with  $\mathbf{1}(\cdot)$  being the indicator function. To estimate the HMRF parameters  $\Phi = \{\phi, \varphi\}$ ,  $(\Theta, \mathbf{K}, \mathbf{X})$  are used as the complete data variables to construct the auxiliary function in the  $(t + 1)$ st iteration of EM algorithm given the observed data  $\mathbf{x}$  and the current estimated parameters  $\Phi^{(t)}$ :

$$Q(\Phi|\Phi^{(t)}) = E_{\Phi^{(t)}}[\log P_{\Phi}(\Theta, \mathbf{K}, \mathbf{X})|\mathbf{x}], \quad (8)$$

where  $P_{\Phi}(\Theta, \mathbf{K}, \mathbf{X}) = P_{\varphi}(\Theta)P_{\phi}(\mathbf{X}, \mathbf{K}|\Theta) = P_{\varphi}(\Theta) \prod_{s \in S} P_{\phi}(X_s, K_s|\Theta_s)$ . The  $Q$ -function can be further written as follows

$$Q(\Phi|\Phi^{(t)}) = Q_1(\phi|\Phi^{(t)}) + Q_2(\varphi|\Phi^{(t)}),$$

where

$$Q_1(\phi|\Phi^{(t)}) = \sum_{\Theta} \sum_{\mathbf{K}} P_{\Phi^{(t)}}(\Theta, \mathbf{K}|\mathbf{x}) \log P_{\phi}(\mathbf{x}, \mathbf{K}|\Theta) \quad (9)$$

and

$$Q_2(\varphi|\Phi^{(t)}) = \sum_{\Theta} P_{\Phi^{(t)}}(\Theta|\mathbf{x}) \log P_{\varphi}(\Theta). \quad (10)$$

Therefore, we can maximize  $Q(\Phi|\Phi^{(t)})$  for  $\Phi$  by maximizing  $Q_1(\phi|\Phi^{(t)})$  for  $\phi$  and  $Q_2(\varphi|\Phi^{(t)})$  for  $\varphi$ , separately.

Maximizing  $Q_1(\phi|\Phi^{(t)})$  under the constraint  $\sum_l p_l = 1$  by the method of Lagrange multipliers yields

$$p_l^{(t+1)} = \frac{\sum_{s \in S} w_s^{(t)}(l)}{\sum_{s \in S} \gamma_s^{(t)}(1)}, \quad (11)$$

$$\mu_l^{(t+1)} = \frac{\sum_{s \in S} w_s^{(t)}(l) x_s}{\sum_{s \in S} w_s^{(t)}(l)}, \quad (12)$$

$$(\sigma_l^2)^{(t+1)} = \frac{\sum_{s \in S} w_s^{(t)}(l) (x_s - \mu_l^{(t+1)})^2}{\sum_{s \in S} w_s^{(t)}(l)}, \quad (13)$$

where

$$\begin{aligned} w_s(l) &= \frac{\gamma_s(1) p_l f_l(x_s)}{f(x_s)}, \\ \gamma_s(i) &= P_{\Phi}(\Theta_s = i|\mathbf{x}), \\ f_l &= N(\mu_l, \sigma_l^2), \quad \text{and } f = \sum_l p_l f_l. \end{aligned}$$

For  $Q_2(\varphi|\Phi^{(t)})$ , taking its first and second derivatives with respect to  $\varphi$ , we obtain

$$\begin{aligned} U^{(t+1)}(\varphi) &= \frac{\partial}{\partial \varphi} Q_2(\varphi|\Phi^{(t)}) \\ &= E_{\Phi^{(t)}}[H(\Theta)|\mathbf{x}] - E_{\varphi}[H(\Theta)], \end{aligned} \quad (14)$$

$$I(\varphi) = -\frac{\partial^2}{\partial \varphi \partial \varphi^T} Q_2(\varphi|\Phi^{(t)}) = \text{Var}_{\varphi}[H(\Theta)]. \quad (15)$$

Maximizing  $Q_2(\varphi|\Phi^{(t)})$  is then equivalent to solving the nonlinear equation:

$$U^{(t+1)}(\varphi) = E_{\Phi^{(t)}}[H(\Theta)|\mathbf{x}] - E_{\varphi}[H(\Theta)] = 0. \quad (16)$$

It can be shown that equation (16) has a unique solution and can be solved by the Newton-Raphson (NR) method (Stoer and Bulirsch 2002). However, a starting point that is not close enough to the solution may result in divergence of the NR method. Therefore, rather than searching for the solution of equation (16) over all  $\varphi$ , we choose a  $\varphi^{(t+1)}$  that increases  $Q_2(\varphi|\Phi^{(t)})$  over its value at  $\varphi = \varphi^{(t)}$ . Together with the maximization of  $Q_1(\phi|\Phi^{(t)})$ , the approach leads to  $Q(\Phi^{(t+1)}|\Phi^{(t)}) \geq Q(\Phi^{(t)}|\Phi^{(t)})$ , which is termed a generalized EM (GEM) algorithm (Dempster et al. 1977). To find such a  $\varphi^{(t+1)}$  that increases the  $Q_2$ -function, a backtracking line search algorithm (Nocedal and Wright 2006) is applied with a set of decreasing positive values  $\lambda_m$  in the following

$$\varphi^{(t+1,m)} = \varphi^{(t)} + \lambda_m I(\varphi^{(t)})^{-1} U^{(t+1)}(\varphi^{(t)}), \quad (17)$$

where  $m = 0, 1, \dots$ , and  $\varphi^{(t+1)} = \varphi^{(t+1,m)}$  which is the first one satisfying the Armijo condition (Nocedal and Wright 2006)

$$\begin{aligned} &Q_2(\varphi^{(t+1,m)}|\Phi^{(t)}) - Q_2(\varphi^{(t)}|\Phi^{(t)}) \\ &\geq \alpha \lambda_m U^{(t+1)}(\varphi^{(t)})^T I(\varphi^{(t)})^{-1} U^{(t+1)}(\varphi^{(t)}). \end{aligned} \quad (18)$$

Since  $I(\varphi^{(t)})$  is positive-definite, the Armijo condition guarantees the increase of  $Q_2$ -function. In practice,  $\alpha$  is chosen to be quite small. We adopt  $\alpha = 10^{-4}$ , which is recommended by Nocedal and Wright (2006), and halve the Newton-Raphson step length each time by using  $\lambda_m = 2^{-m}$ . By the ergodic theorem of the Gibbs sampler (Roberts and Smith 1994),

$$\begin{aligned} U^{(t+1)}(\varphi) &\approx \frac{1}{n} \sum_{i=1}^n \left( H(\boldsymbol{\theta}^{(t,i,\mathbf{x})}) - H(\boldsymbol{\theta}^{(i,\varphi)}) \right), \\ I(\varphi) &\approx \frac{1}{n-1} \sum_{i=1}^n \left( H(\boldsymbol{\theta}^{(i,\varphi)}) - \frac{1}{n} \sum_{j=1}^n H(\boldsymbol{\theta}^{(j,\varphi)}) \right)^{\otimes 2}, \end{aligned}$$

where  $\{\boldsymbol{\theta}^{(t,1,\mathbf{x})}, \dots, \boldsymbol{\theta}^{(t,n,\mathbf{x})}\}$  are large  $n$  samples generated by the Gibbs sampler from

$$P_{\Phi^{(t)}}(\boldsymbol{\theta}|\mathbf{x}) = \frac{\exp\left\{\beta^{(t)} \sum_{\langle s,r \rangle} \theta_s \theta_r + \sum_{s \in S} h_s^{(t)} \theta_s\right\}}{Z\left(\beta^{(t)}, \{h_s^{(t)}\}_{s \in S}\right)},$$

with

$$h_s^{(t)} = h^{(t)} + \frac{(x_s - \mu_0)^2}{2\sigma_0^2} + \frac{1}{2} \log(2\pi\sigma_0^2) \\ + \log\left(\sum_{l=1}^L \frac{p_l^{(t)}}{\sqrt{2\pi\sigma_l^2}} \exp\left\{-\frac{(x_s - \mu_l^{(t)})^2}{2\sigma_l^2}\right\}\right)$$

and  $Z\left(\beta^{(t)}, \{h_s^{(t)}\}_{s \in S}\right)$  being the normalizing constant, and  $\{\boldsymbol{\theta}^{(1,\varphi)}, \dots, \boldsymbol{\theta}^{(n,\varphi)}\}$  are generated from  $P_\varphi(\boldsymbol{\theta})$ . Here for vector  $v$ ,  $v^{\otimes 2} = vv^T$ . Similarly,

$$\frac{C}{Z(\varphi)} = E_\varphi[\exp\{-\varphi^T H(\boldsymbol{\Theta})\}] \\ \approx \frac{1}{n} \sum_{i=1}^n \exp\{-\varphi^T H(\boldsymbol{\theta}^{(i,\varphi)})\},$$

where  $C$  is the number of all possible configurations  $\boldsymbol{\theta}$  of  $\boldsymbol{\Theta}$ . Then the difference between  $Q_2$ -functions in the Armijo condition can be approximated by

$$Q_2(\varphi^{(t+1,m)}|\Phi^{(t)}) - Q_2(\varphi^{(t)}|\Phi^{(t)}) \\ \approx \frac{1}{n} (\varphi^{(t+1,m)} - \varphi^{(t)})^T \sum_{i=1}^n H(\boldsymbol{\theta}^{(t,i,\mathbf{x})}) \\ + \log\left(\frac{\sum_{i=1}^n \exp\{-\varphi^{(t+1,m)T} H(\boldsymbol{\theta}^{(i,\varphi^{(t+1,m)})})\}}{\sum_{i=1}^n \exp\{-\varphi^{(t)T} H(\boldsymbol{\theta}^{(i,\varphi^{(t)})})\}}\right).$$

Readers interested in simulating the normalizing constant  $Z(\varphi)$  are referred to the work of Gelman and Meng (1998). Back to  $Q_1(\phi|\Phi^{(t)})$ , the local conditional probability of  $\boldsymbol{\Theta}$  given  $\mathbf{x}$  can also be approximated by the Gibbs sampler:

$$\gamma_s^{(t)}(i) = P_{\Phi^{(t)}}(\Theta_s = i|\mathbf{x}) \\ \approx \frac{1}{n} \sum_{k=1}^n \mathbf{1}(\theta_s^{(t,k,\mathbf{x})} = i). \quad (19)$$

When the number of components in the nonnull mixture  $L \geq 2$ , if  $\mu_l = x_s$  and  $\sigma_l^2 \rightarrow 0$  for some mixture component  $l$  and a voxel  $s$  with other parameters fixed, then

the likelihood function  $L(\Phi|\mathbf{x}) = P_{\Phi}(\mathbf{x}) \rightarrow \infty$ . One solution to avoid the degeneracy of the likelihood function is to replace the likelihood function by a penalized likelihood function (Ridolfi 1997; Ciuperca et al. 2003)

$$pL(\Phi|\mathbf{x}) = L(\Phi|\mathbf{x}) \prod_{l=1}^L g(\sigma_l^2),$$

where  $g$  is a proper probability density function that yields similar results with (11), (12) and (13). We choose  $g(\sigma_l^2)$  to be the inverse gamma distribution, i.e,

$$g(\sigma_l^2) = \frac{a^{b-1}}{\Gamma(b-1)} \frac{1}{\sigma_l^{2b}} \exp \left\{ -\frac{a}{\sigma_l^2} \right\},$$

where  $a > 0, b > 1$ . For a finite mixture of normal distributions, the penalized maximum likelihood estimator (PMLE) based on the inverse gamma distribution as the penalty function has strong consistency and asymptotic normality (Ciuperca et al. 2003; Chen et al. 2008), therefore we think the inverse gamma distribution would be a reasonable choice for our model, which performs well in our simulations. Formal proofs of consistency and asymptotic normality are still open questions. The penalized likelihood approach is equivalent to setting  $g(\sigma_l^2)$  to be the prior distribution for each  $\sigma_l^2$ , leading to the auxiliary function for the penalized EM algorithm as follows:

$$\begin{aligned} Q(\Phi|\Phi^{(t)}) &= \sum_{\Theta} \sum_{\mathbf{K}} P_{\Phi^{(t)}}(\Theta, \mathbf{K}|\mathbf{x}) \\ &\quad \times \log \left( P_{\Phi}(\Theta, \mathbf{K}, \mathbf{x}) \prod_{l=1}^L g(\sigma_l^2) \right) \\ &= Q_1(\phi|\Phi^{(t)}) + Q_2(\varphi|\Phi^{(t)}), \end{aligned}$$

where

$$\begin{aligned} Q_1(\phi|\Phi^{(t)}) &= \sum_{\Theta} \sum_{\mathbf{K}} P_{\Phi^{(t)}}(\Theta, \mathbf{K}|\mathbf{x}) \\ &\quad \times \log \left( P_{\phi}(\mathbf{x}, \mathbf{K}|\Theta) \prod_{l=1}^L g(\sigma_l^2) \right), \end{aligned}$$

and  $Q_2(\varphi|\Phi^{(t)})$  is the same as equation (10). Then only equation (13) becomes

$$(\sigma_l^2)^{(t+1)} = \frac{2a + \sum_{s \in S} w_s^{(t)}(l) (x_s - \mu_l^{(t+1)})^2}{2b + \sum_{s \in S} w_s^{(t)}(l)} \quad (20)$$

and equations (11) and (12) for other parameters remain unchanged.

### 3.2 Implementation of the LIS-Based FDR Procedure

The algorithm for the LIS-based data-driven procedure, denoted as LIS for single group analysis, SLIS for separate analysis of multiple groups, and PLIS for pooled analysis for multiple groups, is given below:

1. Set initial values  $\Phi^{(0)} = \{\phi^{(0)}, \varphi^{(0)}\}$  for the model parameters  $\Phi$  of each group;
2. Update  $\phi^{(t)}$  from equations (11), (12) and (13) for  $L = 1$  or (20) for  $L \geq 2$ ;
3. Update  $\varphi^{(t)}$  from equations (17) and (18);
4. Iterate Steps 2 and 3 until convergence, then obtain the estimate  $\hat{\Phi}$  of  $\Phi$ ;
5. Plug-in  $\hat{\Phi}$  to obtain the test statistics  $\widehat{LIS}$  from equation (19);
6. Apply the data-driven procedure (LIS, SLIS or PLIS).

The GEM algorithm is stopped when the following stopping rule

$$\max_i \left( \frac{|\Phi_i^{(t+1)} - \Phi_i^{(t)}|}{|\Phi_i^{(t)}| + \epsilon_1} \right) < \epsilon_2, \quad (21)$$

where  $\Phi_i$  is the  $i$ th coordinate of vector  $\Phi$ , is satisfied for three consecutive regular Newton-Raphson iterations with  $m = 0$  in (17), or the pre-specified maximum number of iterations is reached.

Stopping rule (21) was applied by Booth and Hobert (1999) to the Monte Carlo EM method, where they set  $\epsilon_1 = 0.001$ ,  $\epsilon_2$  between 0.002 and 0.005, and the rule to be satisfied for three consecutive iterations to avoid stopping the algorithm prematurely because of Monte Carlo error. We used  $\epsilon_1 = \epsilon_2 = 0.001$  in simulation studies and real-data analysis. Constant  $\alpha = 10^{-4}$  is recommended by Nocedal and Wright (2006) for the Armijo condition (18), and the Newton-Raphson step length in (17) is halved by using  $\lambda_m = 2^{-m}$ . In practice, the Armijo condition (18) might not be satisfied when the step length  $\|\varphi^{(t+1,m)} - \varphi^{(t)}\|$  is very small. In this situation, the iteration within Step 3 is stopped by an alternative criterion

$$\max_i \left( \frac{|\varphi_i^{(t+1,m)} - \varphi_i^{(t)}|}{|\varphi_i^{(t)}| + \epsilon_1} \right) < \epsilon_3$$

with  $\epsilon_3 < \epsilon_2$ , for example,  $\epsilon_3 = 10^{-4}$  if  $\epsilon_2 = 0.001$ . When  $L \geq 2$ , small  $a$  and  $b$  should be chosen in (20). We choose  $a = 1$  and  $b = 2$ .

## 4. SIMULATION STUDIES

The simulation setups are similar to those in Sun and Cai (2009) and Wei et al. (2009), but with three-dimensional data to mimic brain images. The performance of the proposed LIS-based oracle (OR) and data-driven FDR procedures are compared with the BH approach (Benjamini and Hochberg 1995) and the Lfdr procedure (Sun and Cai 2007) for single group analysis, and with the CLfdr procedure (Cai and Sun 2009) for multiple groups.

The BH procedure is implemented globally for the multiple-group simulation. For the Lfdr or CLfdr procedure, we use the proportion of the null cases generated from the Ising model with given parameters as the estimate of the probability of the null cases  $P(\Theta_s = 0)$ , together with the given null and nonnull distributions without estimating their parameters. For the LIS-based data-driven procedures, the maximum number of GEM iterations is set to be 1,000 with  $\epsilon_1 = \epsilon_2 = 0.001$ ,  $\epsilon_3 = \alpha = 10^{-4}$ ,  $a = 1$  and  $b = 2$ . For the Gibbs sampler (Roberts and Smith 1994; Gilk et al. 1996), 5,000 samples are generated from 5,000 iterations after a burn-in period of 1,000 iterations. In all simulations, each HMRF is on a  $N = 15 \times 15 \times 15$  cubic lattice  $S$ , the number of replications  $M = 200$  is the same as that in Wei et al. (2009), and the nominal FDR level is set at 0.10.

### 4.1 Single-Group Analysis

#### 4.1.1 Study 1: $L = 1$

The MRF  $\Theta = \{\Theta_s : s \in S\}$  is generated from the Ising model (1) with parameters  $(\beta, h)$ , and the observations  $\mathbf{X} = \{X_s : s \in S\}$  are generated conditionally on  $\Theta$  from  $X_s | \Theta_s \sim (1 - \Theta_s)N(0, 1) + \Theta_s N(\mu_1, \sigma_1^2)$ . Figure 1 shows the comparisons of the performance of BH, Lfdr, OR and LIS. In Figure 1(1a-1c), we fix  $h = -2.5$ , set  $\mu_1 = 2$  and  $\sigma_1^2 = 1$ , and plot FDR, FNR, and the average number of true positives (ATP) yielded by these procedures as functions of  $\beta$ . In Figure 1(2a-2c), we fix  $\beta = 0.8$ , set  $\mu_1 = 2$  and  $\sigma_1^2 = 1$ , and plot FDR, FNR and ATP as functions of  $h$ . In Figure 1(3a-3c), we fix  $\beta = 0.8$  and  $h = -2.5$ , set  $\sigma_1^2 = 1$ , and plot FDR, FNR and ATP as functions of  $\mu_1$ . The initial values for the numerical algorithm are set at  $\beta^{(0)} = h^{(0)} = 0$ ,  $\mu_1^{(0)} = \mu_1 + 1$  and  $\sigma_1^{2(0)} = 2$ .

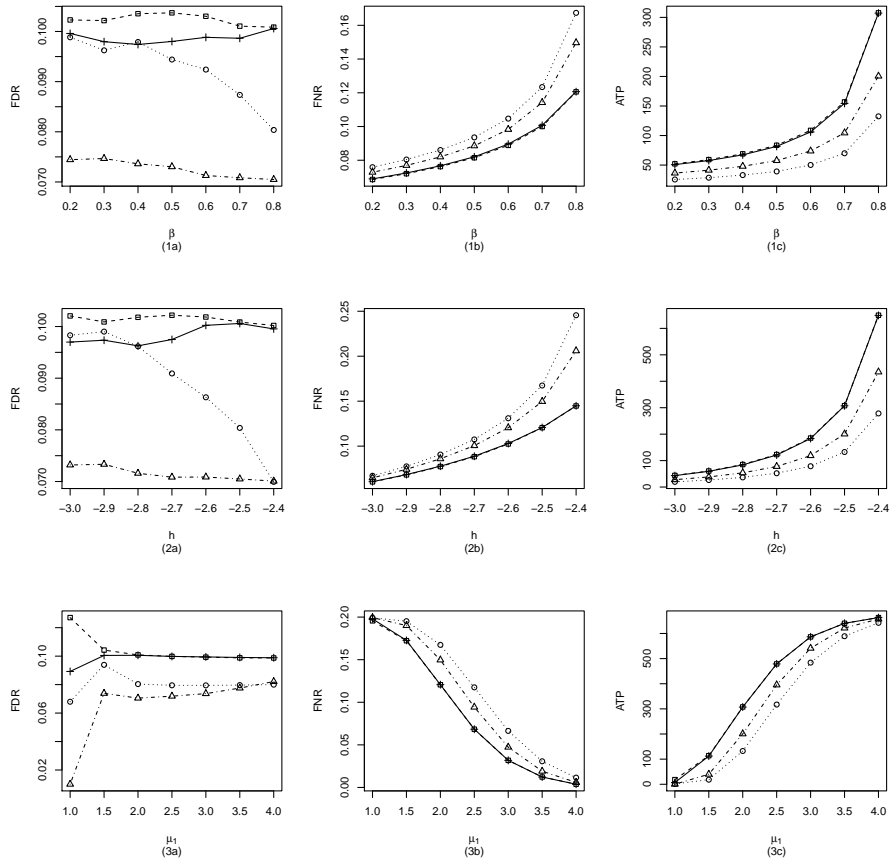


Figure 1. Comparisons of BH ( $\circ$ ), Lfdr ( $\triangle$ ), OR ( $+$ ) and LIS ( $\square$ ) for a single group with  $L = 1$ .

From Figure 1(1a-3a), we can see that the FDR levels of all four procedures are controlled around 0.10 except one case of the LIS procedure in Figure 1(3a) with the lowest  $\mu_1$ , whereas the BH and Lfdr procedures are generally conservative. In Figure 1(3a), the obvious deviation of the FDR level from 0.10 by the LIS procedure for the case  $\mu_1 = 1$  is likely caused by the small lattice size  $N$ . As a confirmation, additional simulations by increasing the lattice size  $N$  to  $30 \times 30 \times 30$  yield a FDR of 0.1018 for the same setup. From Figure 1(1b-3b) and (1c-3c) we can see that the two curves of OR and LIS procedures are almost identical, indicating that the data-driven LIS procedure works equally well as the OR procedure. These plots also show that the LIS procedure outperforms the two independent-case procedures (BH and Lfdr), with increased margin of performance in FNR and ATP as  $\beta$  or  $h$  increases or  $\mu_1$  is at a moderate level. Note that from (3) and (4), we can see that  $\beta$  controls how likely the same-state cases cluster together, and  $\beta$  and  $h$  together control the proportion of the aggregation of nonnulls relative to that of nulls.

#### 4.1.2 Study 2: $L = 2$

We now consider the case where the nonnull distribution is a mixture of two normal distributions. The MRF is generated from the Ising model (1) with fixed parameters  $\beta = 0.8$  and  $h = -2.5$ . The nonnull distribution is a two-component normal mixture  $p_1 N(\mu_1, \sigma_1^2) + p_2 N(\mu_2, \sigma_2^2)$  with fixed  $p_1 = p_2 = 0.5$ ,  $\mu_2 = 2$ , and  $\sigma_1^2 = \sigma_2^2 = 1$ , whereas  $\mu_1$  varies from -4 to -1 with increments of size 0.5 for generating different simulation data sets. The initial values are set at  $\beta^{(0)} = h^{(0)} = 0$ ,  $p_1^{(0)} = 1 - p_2^{(0)} = 0.3$ ,  $\mu_l^{(0)} = \mu_l + 1$ , and  $\sigma_l^{2(0)} = 2, l = 1, 2$ .

The simulation results are summarized in Figure 2. Similar to Figure 1, we can see that all the procedures are controlled around 0.10, where BH and Lfdr are conservative, and OR and LIS perform similarly and outperform both BH and Lfdr procedures.

The results from both simulation studies are very similar to that in Sun and Cai (2009) for the one-dimensional case using HMC. It is clearly seen that, for dependent tests, incorporating dependence structure into a multiple-testing procedure improves efficiency dramatically.



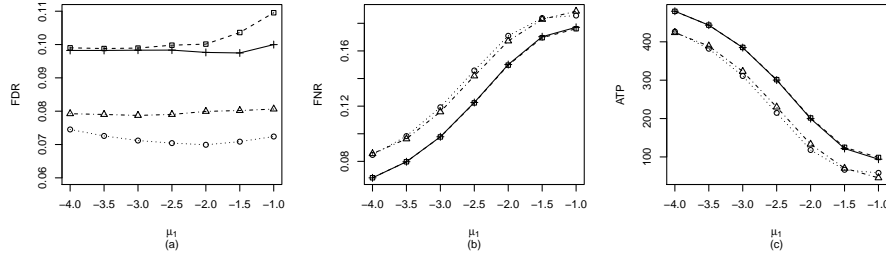


Figure 2. Comparisons of BH ( $\circ$ ), Lfdr ( $\triangle$ ), OR ( $+$ ) and LIS ( $\square$ ) for a single group with  $L = 2$ .

## 4.2 Multiple-Group Analysis

Voxels in a human brain can be naturally grouped into multiple functional regions. For simulations with grouped multiple tests, we consider two lattice groups each with size  $15 \times 15 \times 15$ . The corresponding MRFs  $\Theta_1 = \{\Theta_{1s} : s \in S\}$  and  $\Theta_2 = \{\Theta_{2s} : s \in S\}$  are generated from the Ising model (1) with parameters  $(\beta_1 = 0.2, h_1 = -1)$  and  $(\beta_2 = 0.8, h_2 = -2.5)$ , respectively. The observations  $\mathbf{X}_k = \{X_{ks}, s \in S\}$  are generated conditionally on  $\Theta_k$ ,  $k = 1, 2$ , from  $X_{ks} | \Theta_{ks} \sim (1 - \Theta_{ks})N(0, 1) + \Theta_{ks}N(\mu_k, \sigma_k^2)$ , where  $\mu_1$  varies from 1 to 4 with increments of size 0.5,  $\mu_2 = \mu_1 + 1$  and  $\sigma_1^2 = \sigma_2^2 = 1$ . The initial values are  $\beta_1^{(0)} = \beta_2^{(0)} = h_1^{(0)} = h_2^{(0)} = 0$ ,  $\mu_2^{(0)} = \mu_1^{(0)} = \mu_1 + 1$ , and  $\sigma_1^{2(0)} = \sigma_2^{2(0)} = 2$ .

The simulation results are presented in Figure 3, which are similar to that in Wei et al. (2009) for the one-dimensional case with multiple groups using HMCs. Figure 3(a) shows that all procedures are valid, whereas BH and CLfdr procedures are conservative. We also plot the within-group FDR levels of PLIS for each group separately. One can see that in order to minimize the global FNR level, the PLIS procedure may automatically adjust the FDRs of each individual group, either inflated or deflated reflecting the group heterogeneity, while the global FDR is appropriately controlled. In Figure 3(b) and (c) we see that both SLIS and PLIS outperform the BH and CLfdr procedures, indicating that utilizing the dependency information can improve the efficiency of a testing procedure, and the improvement is more evident for weaker signals (smaller values of  $\mu_1$ ). Between the two LIS-based procedures, PLIS slightly outperforms SLIS, indicating the benefit of ranking the LIS test statistics globally. Particularly, PLIS finds 8.3% more ATP than SLIS when  $\mu_1 = 1$ .

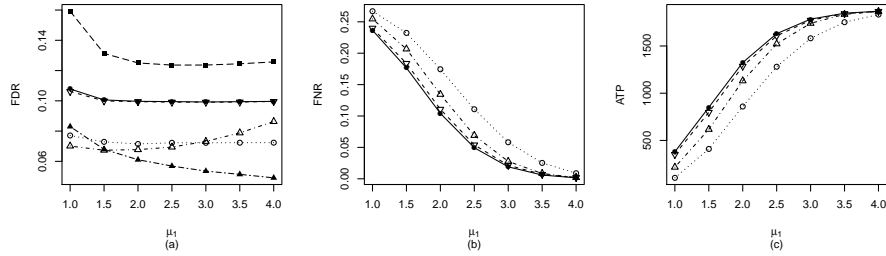


Figure 3. Comparison of BH ( $\circ$ ), CLfdr ( $\triangle$ ), SLIS ( $\nabla$ ) and PLIS ( $\bullet$ ) for two groups with  $L = 1$ . In (a),  $\blacksquare$  and  $\blacktriangle$  represent the results by PLIS for each individual group; for PLIS, while the global FDR is controlled, individual-group FDRs may vary.

## 5. ADNI FDG-PET IMAGE DATA ANALYSIS

We apply the PLIS procedure with HMRFs to the analysis of FDG-PET image data obtained from the ADNI database, which is compared with the BH and CLfdr procedures. Each image is normalized by the average value of pons and cerebellar vermis. Sixty-one brain regions of interest (ROIs) were included in the analysis, where the number of voxels in each region ranges from 149 to 20,680 with a median of 2,517. The total number of voxels of these 61 ROIs is  $N = 251,500$ . The goal is to identify voxels with different metabolic rates of glucose between AD and NC, AD and MCI, and MCI and NC. We only report the comparison of MCI and NC in this article, which has the weakest signals in general among all three comparisons.

We implement the BH procedure globally for the 61 ROIs, whereas treat each region as a group for the CLfdr and PLIS procedures. The null distribution is assumed to be the standard normal distribution. The nonnull distribution is assumed to be a two-component normal mixture for PLIS. For the BH procedure, a total number of  $N$  two-sample Welch's  $t$ -tests (Welch 1947) are performed, and their corresponding two-sided  $p$ -values are obtained. For the PLIS and CLfdr procedures, the  $z$ -values, converted from the  $t$  statistics by the transformation  $z_i = \Phi^{-1}[G_0(t_i)]$  where  $\Phi$  and  $G_0$  are the cumulative distribution functions of the standard normal and the  $t$  statistic respectively, are used as the observed data  $\mathbf{x}$ . The LIS statistics in the PLIS procedure are approximated by  $10^6$  Gibbs-sampler samples, and the Lfdr statistics in the CLfdr procedure are computed by using the R code of Sun and Cai (2007). All the three testing procedures are controlled at a FDR level of 0.001. The initial values for  $\beta$  and

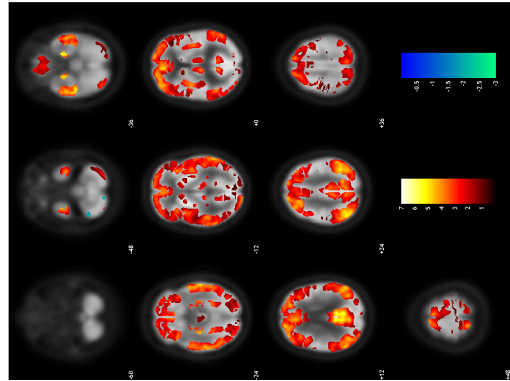
$h$  in the Ising model are set to be zero. The initial values for the nonnull distributions are estimated from the signals claimed by BH at an FDR level of 0.1. The maximum number of GEM iterations is set to be 5,000 with  $\epsilon_1 = \epsilon_2 = 0.001$ ,  $\epsilon_3 = \alpha = 10^{-4}$ ,  $a = 1$  and  $b = 2$ . For the Gibbs sampler embedded in the GEM, 5,000 samples are generated from 5,000 iterations after a burn-in period of 1,000 iterations. In this data analysis, the GEM algorithm reaches the maximum iteration and is then claimed to be converged for five ROIs.

Table 1. Number of voxels with different glucose metabolic rates in MCI comparing with NC found by BH, CLfdr and PLIS procedures

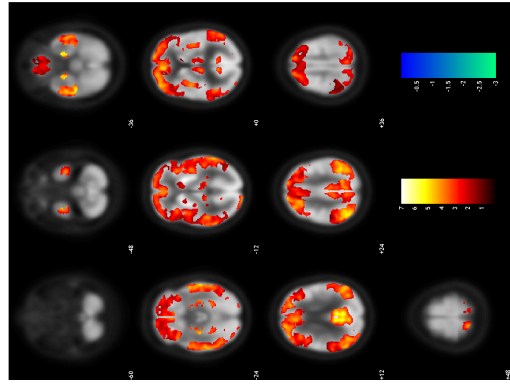
Method	Number of voxels
PLIS	146,867
CLfdr	122,899
BH	8,541
signal by PLIS, noise by CLfdr	34,445
noise by PLIS, signal by CLfdr	10,477
signal by PLIS, noise by BH	138,332
noise by PLIS, signal by BH	6
signal by CLfdr, noise by BH	114,370
noise by CLfdr, signal by BH	12

The results are summarized in Figure 4, where the  $z$ -values for all the signals found by each procedure are plotted. Table 1 summarizes the number of voxels that are claimed as signals by each procedure. We can see that PLIS finds the most number of signals and covers 91.5% and 99.9% of signals detected by CLfdr and BH. It is interesting that the PLIS procedure finds more than 17 times as many signals as the BH procedure, and about 20% more signals than the CLfdr procedure.

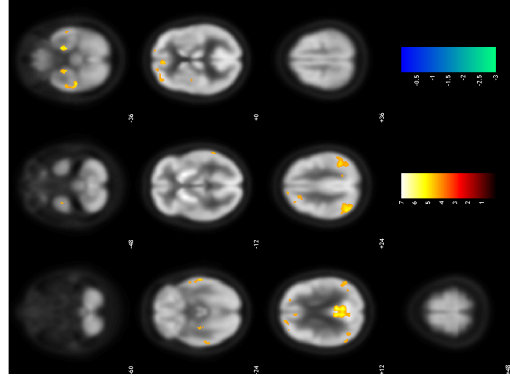
Since the FDG scans were normalized to the average of pons and cerebellar vermis, areas of the brain known to be least affected in AD, it was not surprising that almost all the signals are found with decreased CMRgl. Both PLIS and CLfdr procedures discovered significant metabolic reduction clustered (with a regional proportion of signals  $> 50\%$ ) in brain regions preferentially affected by AD, including the posterior cingulate (Mosconi et al. 2008; Langbaum et al. 2009), parietal cortex (Minoshima et al. 1995; Matsuda 2001), temporal cortex (Alexander et al. 2002; Landau et al. 2011), medial temporal cortex (Karow et al. 2010), frontal cortex (Mosconi 2005), insular cortex (Pernecky et al. 2007), amygdala (Nestor et al. 2003; Gray et al. 2012) and



(a) PLIS



(b) CLfdr



(c) BH

Figure 4. Signals found by each multiple testing procedure. The plotted values are the  $z$ -values for the CMRgl reduction of MCI comparing to NC.

hippocampus (Mosconi et al. 2005). In regions also typically affected in AD, such as anterior cingulate (Fouquet et al. 2009) and occipital cortex (Langbaum et al. 2009), the proportions of signals found by PLIS are 49.6% and 39.0%, respectively, compared with 35.4% and 11.6% found by CLfdr as well as only 1.24% and 0.87% by BH.

With respect to the regions that are relatively spared from AD (Benson et al. 1983; Matsuda 2001; Ishii 2002) or rarely reported in the literature of the disease, caudate, thalamus and putamen are found with high proportions of signals by PLIS ( $> 45\%$ ) and CLfdr ( $> 25\%$ ) in each of these regions; signals in medulla, midbrain, cerebellar hemispheres, pre-motor cortex and primary somatosensory cortex are each claimed with a proportion greater than 20% by PLIS, but very sparse found by both CLfdr and BH. Since MCI as a group consists of a mix of patients, many of them will progress to AD but some will not which may include subjects with corticobasal degeneration (Ishii 2002), frontotemporal dementia (Jeong et al. 2005), or Parkinsonism (Huang et al. 2007; Zeman et al. 2011; Ishii 2013), it is not surprising that some areas not typical of AD patients were found to be abnormal in the MCI group.

## REFERENCES

- Alexander, G. E., Chen, K., Pietrini, P., Rapoport, S. I., and Reiman, E. M. (2002), "Longitudinal PET Evaluation of Cerebral Metabolic Decline in Dementia: A Potential Outcome Measure in Alzheimers Disease Treatment Studies," *American Journal of Psychiatry*, 159, 738-745.
- Benjamini, Y., and Heller, R. (2007), "False Discovery Rates for Spatial Signals," *Journal of the American Statistical Association*, 102, 1272-1281.
- Benjamini, Y., and Hochberg, Y. (1995), "Controlling the False Discovery Rate: A Practical and Powerful Approach to Multiple Testing," *Journal of the Royal Statistical Society, Series B*, 57, 289-300.
- (2000), "On the Adaptive Control of the False Discovery Rate in Multiple Testing with Independent Statistics," *Journal of Educational and Behavioral Statistics*, 25, 60-83.
- Benjamini, Y., and Yekutieli, D. (2001), "The Control of the False Discovery Rate in Multiple Testing under Dependency," *The Annals of Statistics*, 29, 1165-1188.
- Benson, D. F., Kuhl, D. E., Hawkins, R. A., Phelps, M. E., Cummings, J. L., and Tsai, S. Y. (1983), "The Fluorodeoxyglucose 18F Scan in Alzheimer's Disease and Multi-infarct Dementia," *Archives of Neurology*, 40, 711-714
- Besag, J. (1974), "Spatial Interaction and the Statistical Analysis of Lattice Systems,"

- Journal of the Royal Statistical Society*, Series B, 36, 192-236.
- Booth, J. G., and Hobert, J. P. (1999), “Maximizing Generalized Linear Mixed Model Likelihoods with An Automated Monte Carlo EM Algorithm,” *Journal of the Royal Statistical Society*, Series B, 61, 265-285.
- Bremaud, P. (1999), *Markov Chains: Gibbs Fields, Monte Carlo Simulation, and Queues*, New York: Springer.
- Brookmeyer, R., Johnson, E., Ziegler-Graham, K., and Arrighi, H. M. (2007), “Forecasting the Global Burden of Alzheimers Disease,” *Alzheimers & Dementia*, 3, 186-191.
- Cai, T., and Sun, W. (2009), “Simultaneous Testing of Grouped Hypotheses: Finding Needles in Multiple Haystacks,” *Journal of the American Statistical Association*, 104, 1467-1481.
- Chalmond, B. (1989), “An Iterative Gibbsian Technique for Reconstruction of M-ary Images,” *Pattern Recognition*, 22, 747-761.
- Chandgotia, N., Han, G., Marcus, B., Meyerovitch, T., and Pavlov, R. (2014), “One-Dimensional Markov Random Fields, Markov Chains and Topological Markov Fields,” *Proceedings of the American Mathematical Society*, 142, 227-242.
- Chandler, D. (1987), *Introduction to Modern Statistical Mechanics*, New York: Oxford University Press.
- Chen, J., Tan, X., and Zhang, R. (2008), “Inference for Normal Mixtures in Mean and Variance,” *Statistica Sinica*, 18, 443-465.
- Chumbley, J. R., and Friston, K. J. (2009), “False Discovery Rate Revisited: FDR and Topological Inference Using Gaussian Random Fields,” *NeuroImage*, 44, 62-70.
- Chumbley, J., Worsley, K., Flandin, G., and Friston, K. (2010), “Topological FDR for Neuroimaging,” *NeuroImage*, 49, 3057-3064.
- Ciuperca, G., Ridolfi, A., and Idier, J. (2003), “Penalized maximum likelihood estimator for normal mixtures,” *Scandinavian Journal of Statistics*, 30, 45-59.
- Dempster, A. P., Laird, N. M., and Rubin, D. B. (1977), “Maximum Likelihood from Incomplete Data via the EM Algorithm,” *Journal of the Royal Statistical Society*, Series B, 39, 1-38.
- Efron, B. (2004), “Large-Scale Simultaneous Hypothesis Testing: The Choice of a Null Hypothesis,” *Journal of the American Statistical Association*, 99, 96-104.
- (2007), “Size, Power and False Discovery Rates,” *Annals of Statistics*, 35, 1351-1377.
- Farcomeni, A. (2007), “Some Results on the Control of the False Discovery Rate under Dependence,” *Scandinavian Journal of Statistics*, 34, 275-297.
- Fouquet, M., Desgranges, B., Landeau, B., Duchesnay, E., Mezenge, F., De La Sayette, V., Viader, F., Baron, J. C., Eustache, F., and Chetelat, G. (2009), “Longitudinal Brain Metabolic Changes From Amnesic Mild Cognitive Impairment to Alzheimer’s Disease,” *Brain*, 132, 2058-2067.
- Garey, L. J. (2006), *Brodmann’s Localisation in the Cerebral Cortex*, New York: Springer.
- Gelman, A., and Meng X. L. (1998), “Simulating Normalizing Constants: From Importance

- Sampling to Bridge Sampling to Path Sampling,” *Statistical Science*, 13, 163-185.
- Geman, S., and Geman, D. (1984), “Stochastic Relaxation, Gibbs Distributions, and the Bayesian Restoration of Images,” *IEEE Transactions on Pattern Analysis and Machine Intelligence*, 6, 721-741.
- Genovese, C. R., Lazar, N. A., and Nichols, T. (2002), “Thresholding of Statistical Maps in Functional Neuroimaging Using the False Discovery Rate,” *NeuroImage*, 15, 870-878.
- Genovese, C. R., Roeder, K., and Wasserman, L. (2006), “False Discovery Control with p-Value Weighting,” *Biometrika*, 93, 509-524.
- Genovese, C., and Wasserman, L. (2002), “Operating Characteristics and Extensions of the False Discovery Rate Procedure,” *Journal of the Royal Statistical Society, Series B*, 64, 499-517.
- (2004), “A Stochastic Process Approach to False Discovery Control,” *The Annals of Statistics*, 32, 1035-1061.
- Geyer, C. J., and Thompson E. A. (1992), “Constrained Monte Carlo Maximum Likelihood for Dependent Data,” *Journal of the Royal Statistical Society, Series B*, 54, 657-699.
- Gilk, W. R., Richardson, S., and Spiegelhalter, D. J. (eds.) (1996), *Markov Chain Monte Carlo in Practice*, London : Chapman & Hall.
- Gray, K. R., Wolz, R., Heckemann, R. A., Aljabar, P., Hammers, A., and Rueckert, D. (2012), “Multi-Region Analysis of Longitudinal FDG-PET for the Classification of Alzheimer’s Disease,” *NeuroImage*, 60, 221-229.
- Ishii, K. (2002), “Clinical Application of Positron Emission Tomography for Diagnosis of Dementia,” *Annals of Nuclear Medicine*, 16, 515-525.
- (2013), “PET Approaches for Diagnosis of Dementia,” *American Journal of Neuro-radiology* [online], DOI: 10.3174/ajnr.A3695. Available at <http://dx.doi.org/10.3174/ajnr.A3695>.
- Jeong, Y., Cho, S. S., Park, J. M., Kang, S. J., Lee, J. S., Kang, E., Na, D. L., and Kim, S. E. (2005), “18F-FDG PET Findings in Frontotemporal Dementia: An SPM Analysis of 29 Patients,” *Journal of Nuclear Medicine*, 46, 233-239.
- Karow, D. S., McEvoy, L. K., Fennema-Notestine, C., Hagler, D. J., Jennings, R. G., Brewer, J. B., Hoh, C. K., and Dale, A. M. (2010), “Relative Capability of MR Imaging and FDG PET to Depict Changes Associated with Prodromal and Early Alzheimer Disease,” *Radiology*, 256, 932-942.
- Landau, S. M., Harvey, D., Madison, C. M., Koeppe, R. A., Reiman, E. M., Foster, N. L., Weiner, M. W., and Jagust, W. J. (2011), “Associations between Cognitive, Functional, and FDG-PET Measures of Decline in AD and MCI,” *Neurobiology of Aging*, 32, 1207-1218.
- Langbaum, J. B. S., Chen, K., Lee, W., Reschke, C., Bandy, D., Fleisher, A. S., Alexander, G. E., Foster, N. L., Weiner, M. W., Koeppe, R. A., Jagust, W. J., and Reiman, E. M. (2009), “Categorical and Correlational Analyses of Baseline Fluorodeoxyglucose Positron Emission Tomography Images from the Alzheimer’s Disease Neuroimaging Initiative (ADNI),” *NeuroImage*, 45, 1107-1116.

- Li, H., Wei, Z., and Maris, J. (2010), “A Hidden Markov Random Field Model for Genome-Wide Association Studies,” *Biostatistics*, 11, 139-150.
- Magder, L. S., and Zeger, S. L., (1996), “A Smooth Nonparametric Estimate of A Mixing Distribution Using Mixtures of Gaussians,” *Journal of the American Statistical Association*, 91, 1141-1151.
- Marroquin, J. L., Santana, E. A., and Botello, S. (2003), “Hidden Markov Measure Field Models for Image Segmentation,” *IEEE Transactions on Pattern Analysis and Machine Intelligence*, 25, 1380-1387.
- Matsuda, H. (2001), “Cerebral Blood Flow and Metabolic Abnormalities in Alzheimers Disease,” *Annals of Nuclear Medicine*, 15, 85-92.
- Minoshima, S., Frey, K. A., Koeppe, R. A., Foster, N. L., and Kuhl, D. E. (1995), “A Diagnostic Approach in Alzheimer’s Disease Using Three-dimensional Stereotactic Surface Projections of Fluorine-18-FDG PET,” *Journal of Nuclear Medicine*, 36, 1238-1248.
- Mosconi, L. (2005), “Brain glucose metabolism in the early and specific diagnosis of Alzheimers disease,” *European Journal of Nuclear Medicine and Molecular Imaging*, 32, 486-510.
- Mosconi, L., Tsui, W. H., De Santi, S., Li, J., Rusinek, H., Convit, A., Li, Y., Boppana, M., and De Leon, M. J. (2005), “Reduced Hippocampal Metabolism in MCI and AD: Automated FDG-PET Image Analysis,” *Neurology*, 64, 1860-1867.
- Mosconi, L., Tsui, W. H., Herholz, K., Pupi, A., Drzezga, A., Lucignani, G., Reiman, E. M., Holthoff, V., Kalbe, E., Sorbi, S., Diehl-Schmid, J., Pernecky, R., Clerici, F., Caselli, R., Beuthien-Baumann, B., Kurz, A., Minoshima, S., and De Leon, M. J. (2008), “Multicenter Standardized 18F-FDG PET Diagnosis of Mild Cognitive Impairment, Alzheimer’s Disease, and Other Dementias,” *Journal of Nuclear Medicine*, 49, 390-398.
- Nestor, P. J., Fryer, T. D., Smielewski, P., and Hodges, J. R. (2003), “Limbic Hypometabolism in Alzheimers Disease and Mild Cognitive Impairment,” *Annals of Neurology*, 54, 343-351.
- Nichols, T., and Hayasaka, S. (2003), “Controlling the Familywise Error Rate in Functional Neuroimaging: a Comparative Review,” *Statistical Methods in Medical Research*, 12, 419-446.
- Nocedal, J., and Wright, S. (2006), *Numerical Optimization* (2nd ed.), New York: Springer.
- Pernecky, R., Drzezga, A., Diehl-Schmid, J., Li, Y., and Kurz, A. (2007), “Gender Differences in Brain Reserve: An (18)F-FDG PET Study in Alzheimers Disease,” *Journal of Neurology*, 254, 1395-1400.
- Ridolfi, A. (1997), “Maximum Likelihood Estimation of Hidden Markov Model Parameters, with Application to Medical Image Segmentation,” Master’s thesis, Politecnico di Milano, Milan, Italy.
- Roberts, G. O., and Smith A. F. M. (1994), “Simple Conditions for the Convergence of the Gibbs Sampler and Metropolis-Hastings Algorithms,” *Stochastic Processes and their Applications*, 49, 207-216.
- Stoer, J., and Bulirsch, R. (2002), *Introduction to Numerical Analysis* (3rd ed.), New York: Springer.



- Sun, W., and Cai, T. T. (2007), “Oracle and Adaptive Compound Decision Rules for False Discovery Rate Control,” *Journal of the American Statistical Association*, 102, 901-912.
- (2009), “Large-Scale Multiple Testing under Dependence,” *Journal of the Royal Statistical Society, Series B*, 71, 393-424.
- Wang, X. (2013), “Regularized Functional Regression Models with Applications to Brain Imaging,” Ph.D. dissertation, University of Michigan, Department of Biostatistics.
- Wei, Z., Sun, W., Wang, K., and Hakonarson, H. (2009), “Multiple Testing in Genome-Wide Association Studies via Hidden Markov Models,” *Bioinformatics*, 25, 2802-2808.
- Welch, B. L. (1947), “The Generalization of ‘Student’s’ Problem when Several Different Population Variances are Involved,” *Biometrika*, 34, 28-35.
- Winkler, G. (2003), *Image Analysis, Random Fields and Markov Chain Monte Carlo Methods* (2nd ed.), New York: Springer.
- Wu, W. B. (2008), “On False Discovery Control under Dependence,” *The Annals of Statistics*, 36, 364-380.
- Yekutieli, D., and Benjamini, Y. (1999), “Resampling-Based False Discovery Rate Controlling Multiple Test Procedures for Correlated Test Statistics,” *Journal of Statistical Planning and Inference*, 82, 171-196.
- Zeman, M. N., Carpenter, G. M., and Scott, P. J. (2011), “Diagnosis of Dementia Using Nuclear Medicine Imaging Modalities,” in *12 Chapters on Nuclear Medicine*, ed. A. Gholamrezanezhad, Croatia: InTech, pp. 199-230.
- Zhang, J. (1992), “The Mean Field Theory in EM Procedures for Markov Random Fields,” *IEEE Transactions on Signal Processing*, 40, 2570-2583.
- Zhu, H., Gu, M., and Peterson, B. (2007), “Maximum Likelihood from Spatial Random Effects Models via the Stochastic Approximation Expectation Maximization Algorithm,” *Statistics and Computing*, 17, 163-177.